Applied Catalysis B: Environmental 158–159 (2014) 321–328

Contents lists available at ScienceDirect

Applied Catalysis B: Environmental

journal homepage: www.elsevier.com/locate/apcatb

Inorganic ions promoted photocatalysis based on polymer photocatalyst

Honglin Gao[a,b], Shicheng Yan[a,c,*], Jiajia Wang[a], Zhigang Zou[a,c]

[a] Eco-Materials and Renewable Energy Research Center (ERERC), College of Engineering and Applied Sciences, Nanjing University, Nanjing 210093, PR China
[b] Research Institute of Engineering and Technology, Yunnan University, Kunming, Yunnan 650091, PR China
[c] Kunshan Innovation Institute of Nanjing University, Kunshan 215300, PR China

ARTICLE INFO

Article history:
Received 22 January 2014
Received in revised form 14 April 2014
Accepted 19 April 2014
Available online 28 April 2014

Keywords:
g-C_3N_4
Sulfite anion
Na^+ cation
Visible light
Photodegradation

ABSTRACT

This paper reports effect of inorganic ions on removal of organic pollutants over the g-C_3N_4 polymer photocatalyst by photocatalysis. The oxidation of SO_3^{2-} by photogenerated hole on g-C_3N_4 will induce a chain reaction initialed by SO_3^{2-} to form •OH while the hole oxidation of SO_3^{2-} increases the separation of photogenerated electron and hole, which process promotes the photogenerated electron induced multistep reduction of O_2 generating •OH to proceed. On the other hand, the cation, Na^+, can interact with the negatively charged nitrogen pots in the C_3N_4 sheets *via* the ion dipole interaction. Such ion dipole interaction significantly improves the charge separation and transport, thus accelerating the formation of active species (•OH). As a result of positive effect of Na^+ and SO_3^{2-} on photocatalysis of g-C_3N_4, the degradation rates of organic pollutants over g-C_3N_4 were significantly increased. Our studies offer the new opportunities for using the g-C_3N_4 with low cost and facile adjustable function to treat industrial wastewater containing organic pollutants.

1. Introduction

Photocatalysis is considered to be an advanced oxidation technique for the remediation of water containing organic pollutants [1–3]. For the purpose of giving full play to solar energy, numerous investigations have been developed to rummage the materials with visible light activities [4,5]. Recently, the free-metal photocatalyst, graphitic carbon nitride (g-C_3N_4) had been developed and investigated widely in the use of visible light for degradation of organic pollutants, splitting water and photocatalytic conversion of CO_2 [6–8]. Several efforts have been devoted to improve the photocatalytic performance of g-C_3N_4 in terms of heteroatoms modification, forming composite, sensitizing by dyes and morphology manipulation [8–15]. However, a challenge is still kept in understanding the interaction between g-C_3N_4 photocatalyst and the reaction species.

From view of practical applications of photocatalysis, the photocatalyst is usually used in a complex environment, which probably contains various ions. The negative effect of inorganic ions such as PO_4^{3-}, NO_3^-, SO_4^{2-}, ClO_4^- and HCO_3^- on the photodegradation of organic pollutants was found during the TiO_2 photocatalysis, due to the competitive adsorption to surface active sites [16]. On the contrary, the addition of oxyanion oxidants such as ClO_2^-, ClO_3^-, IO_4^-, $S_2O_8^-$ and BrO_3^- promoted photocatalytic activity of TiO_2 in removal of organic pollutants by scavenging conduction-band electrons and reducing the charge-carrier recombination [17]. The existing experimental evidences have confirmed that the presence of inorganic ions in water is an important factor to affect the photocatalytic activity of photocatalyst. Sodium sulfite, Na_2SO_3, as an industrial additive agent, was widely used in various industrial fields such as printing and dyeing, photographic, electronic, textile and food industry, meaning that the Na_2SO_3 is a common compound in the industrial wastewater [18,19]. However, there is no report on the effect of Na_2SO_3 on the photodegradation of organic pollutants by photocatalysis.

In this paper, our aim is to investigate the photodegradation of organic pollutants over g-C_3N_4 polymer photocatalyst, which is performed in the Na_2SO_3 aqueous solution. Using a typical azo compound, methyl orange (MO), as the degrading target, we found that the photocatalytic degradation of MO over g-C_3N_4 was significantly improved by addition of Na_2SO_3. Our results indicated that the anion, SO_3^{2-}, can be oxidated to $•SO_3^-$ by photogenerated hole. During the oxidation reaction of SO_3^{2-}, a chain reaction initialed by $•SO_3^-$ occurs and the •OH as an active species forms. In addition, the oxidation of SO_3^{2-} by hole would increase the separation

* Corresponding author at: Eco-Materials and Renewable Energy Research Center (ERERC), College of Engineering and Applied Sciences, Nanjing University, Nanjing 210093, PR China. Tel.: +86 25 83686639; fax: +86 25 83686632.
E-mail addresses: yscfei@nju.edu.cn, yscfei@tom.com (S. Yan).

http://dx.doi.org/10.1016/j.apcatb.2014.04.036
0926-3373/

of photogenerated electron and hole, which process promotes the photogenerated electron induced multistep reduction of O_2 generating •OH to proceed. The cation, Na^+, seems to interact with the negatively charged nitrogen pots in the C_3N_4 sheets, which induces the efficient charge separation and transport, thus accelerating the photodegradation of methyl orange.

2. Experimental

2.1. Preparation of photacalyst

The g-C_3N_4 was prepared by polycondensation of melamine [20]. In a typical run, 6 g of melamine powder was put into an alumina crucible with a cover to prevent sublimation of melamine, and then heated to 500 °C in a muffle furnace for 2 h at a heating rate of 10 °C/min; the further deammonation treatment was performed at 520 °C for 2 h. After cooled to room temperature, the as-synthesized yellow product was milled into a powder.

2.2. Characterization

X-ray powder diffraction (XRD) measurements were performed on a D/MAX-uL TIMA3 X-ray diffractometer, using Cu K_α radiation (λ = 1.5406 Å), with 0.02° 2θ steps from 5 to 60°. Fourier transform infrared (FTIR) spectra were recorded using a Nicolet Nexus 870 FTIR spectrometer. The UV–vis diffuse reflectance spectrum was recorded with a UV-2550 Ultraviolet-visible spectrophotometer at room temperature and transformed to the absorption spectrum according to the Kubelka–Munk relationship. The photoluminescence (PL) spectroscopy was obtained by using the Cary eclipse fluorescence spectrophotometer (USA).

2.3. Photocatalytic tests

The photodegradation experiments by the as-prepared g-C_3N_4 samples were carried out in a Pyrex top irradiation reaction vessel. The light irradiation system contains a 300 W Xe lamp with cutoff filter L42 for visible light and a water filter to keep the temperature at 20 °C. 0.3 g catalyst was dispersed in a methyl orange (MO) aqueous solution (100 mL, 4 mg L^-). In the case of addition of ions, the Na_2SO_3 or Na_2SO_4 was respectively added with concentration of 0.01 mol L^-. The changes in MO concentration were monitored by using UV–vis absorption spectrum (Varian, CARY 50 probe, USA) to measure the remained MO. The degradation efficiency was determined by dividing C/C_0, where C is the remained MO concentration and C_0 is the starting MO concentration.

2.4. Analytic methods

The active species for photodegrading dyes were trapped by a spin trap 5,5-dimethyl-1-pyrroline-N-oxide (DMPO). The preparation procedure of DMPO solution was as follows: for removing oxygen dissolved in water, the deionized water was first heated at 100 °C for 30 min. Then the thus-treated deionized water was used to make the 50 mM DMPO aqueous solution in nitrogen atmosphere in a vacuum glove box. The obtained DMPO solution with an appropriate content of catalyst was loaded into a quartz capillary and irradiated for a given time by using the same light source used in the above photocatalytic reaction. The electron paramagnetic resonance (EPR) spectra were obtained using a Bruker (model EMX-10/12 X-band) electron paramagnetic resonance spectrometer. The settings were center field, 3480.0 G; microwave frequency, 9.2–9.8 GHz; power, 19.97 mW.

Time-resolved fluorescence measurements were performed by using a time-correlated single photon counting (TCSPC) setup with a FM-4P-TCSPC spectrometer (Horiba Jobin Yvon, Paris, France). The excitation wavelength was 350 nm. Raw decay data presented as logarithm of photon counts *vs* time were analyzed with data analysis software of DAS6 (v6.6). The decay times were extracted by means of a reconvolution fit based on a triple exponential model. Considering that fluorescence intensity as a function of time gradually decays to the ground state, which process follows the multi exponential law of

$$I(t) = I_0 \sum_{i=1}^{n} a_i e^{-t/\tau}$$

where t is the decay time after the absorption, $I(t)$ is the fluorescence intensity at time t, I_0 is the intensity at time t = 0, τ is the lifetime and a_i is the pre-exponential factor, the intensity averaged-fluorescence lifetime $\bar{\tau}$ was calculated as

$$\bar{\tau} = \frac{\sum_{i=1}^{n} a_i \tau_i^2}{\sum_{i=1}^{n} a_i \tau_i}$$

PL quantum efficiencies (φ) were determined with a Hamamatsu C9920 set-up, including an integrating sphere combined with a photonic multi-channel analyzer. The nonradiative decay rate (K_{nr}) was determined according to

$$K_{nr} = \frac{1 - \varphi}{\bar{\tau}}$$

Total organic carbon (TOC) was detected on Shimadzu TOC5000 analyzer (Japan). The TOC was calculated by subtracting inorganic carbon from total carbon. The product formed during photodegrading dye was measured by liquid chromatography/mass spectrometry (LC/MS) using Agilent 1290-6460 with electrospray ionization (ESI) interface. Chromatographic separation was carried out at 30 °C with C18 (5 μm × 150 mm × 2.0 mm) column. The mobile phase consisting of acetonitrile/ammonium acetate = 20:80 (V/V) was set at a flow rate of 0.8 mL/min. The ESI source was set at the negative ionization mode. The MS operating conditions were optimized as follows: drying gas flow was 8 L/min, sheath gas temperature was 325 °C, capillary voltage was +3 kV, endplate offset was fixed at 500 V, and the nebulizer pressure was 30 psi. The mass range was from 100 to 400 Da.

3. Results and discussion

The XRD and FTIR analysis indicate that the g-C_3N_4 prepared by heating melamine belongs to a layered solid with *ABA* stacking of graphene-like C—N conjugated sheet, as shown in Fig. S1, which is in good agreement with the previous reports [20]. The photodegradation experiment was performed by dispersing the g-C_3N_4 powders into methyl orange (MO) containing Na_2SO_3 solution (Fig. 1). After 0.5 h visible light irradiation, the main absorbance peak of MO at 464 nm disappeared completely. However, for the mixing solution of MO and g-C_3N_4 without addition of Na_2SO_3, only 34% of peak intensity of MO decreased after the same light irradiation time. This indicates that the addition of Na_2SO_3 significantly improves the conversion of MO. Obviously, the dye adsorption on the surface of g-C_3N_4 was decreased when the ions were added into the reaction solution. Therefore, the increase in photodegradation of MO cannot be attributed to the effect of ions on the dye adsorption.

The active species, which formed during light irradiation, were captured by a spin trap DMPO and detected by EPR. As shown in Fig. 2A, visible light irradiation of DMPO-containing aqueous suspensions of g-C_3N_4 gives rise to exclusively a 1:2:2:1 quartet signal in the EPR spectrum. The EPR parameters (g = 2.0056, α^N = 15.0 G and α^H = 15.0 G) are characteristic of DMPO-•OH adducts formed upon trapping of •OH radicals by the DMPO molecules [21], indicating that hydroxyl radical is the active species for photoirradiated

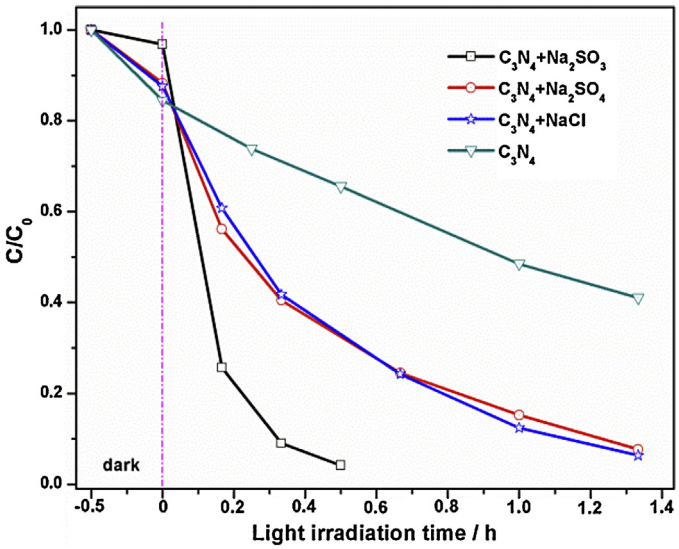

Fig. 1. The MO concentration change by monitoring the main absorbance peak at 464 nm as a function of the light irradiation time under different reaction systems.

g-C_3N_4. Generally, the photodegradating activity of semiconductor photocatalyst is associated with oxidation ability of photogenerated holes in valence band and reduction ability of photogenerated electrons in conduction band. The oxidation potential of valance band of g-C_3N_4 is 1.53 V [22]. Such low oxidation potential means that the photogenerated holes are incapable of directly oxidizing adsorbed hydroxyl groups generating hydroxyl radicals (2.7 V *vs* NHE). The hydroxyl radical would originate from the photogenerated electron induced multi-step reduction of O_2 as follows [23]:

$$O_2 + e^- \rightarrow {}^\bullet O_2^- \quad (1)$$

$${}^\bullet O_2^- + e^- + 2H^+ \rightarrow H_2O_2 \quad (2)$$

$$H_2O_2 + e^- \rightarrow {}^\bullet OH + OH^- \quad (3)$$

It has been confirmed in our previous report that the photodegrading rates of MO increase largely when the 1 mg L^{-1} H_2O_2 was added into the g-C_3N_4 photocatalysis system. No photodegradation of MO was observed during light irradiating the aquatic solutions of H_2O_2 and dye without g-C_3N_4 photocatalyst. Clearly, the improved reaction activity is due to the introduction of H_2O_2, which accelerates the reaction of Eq. (3) [22]. This further confirmed that the hydroxyl radical resulted from the oxygen reduction by photogenerated electrons. For the visible light irradiation of DMPO + Na_2SO_3 + g-C_3N_4 solution, the EPR spectrum presents characteristic of DMPO–${}^\bullet SO_3^-$ radical adduct (g = 2.0054, α^N = 14.7 G and α^H = 16.0 G) [24]. The one-electron redox potential of ${}^\bullet SO_3^-$ radical was determined by cyclic voltammetry to be 0.63 V *vs* NHE at pH 7 [25], which is lower than oxidation potential of g-C_3N_4 (1.53 V) [22]. This indicates that the SO_3^{2-} will be oxidized into ${}^\bullet SO_3^-$ by photogenerated hole on g-C_3N_4 is energetically possible. It has been demonstrated that the SO_3^{2-} can be used as a hole scavenger for hydrogen production [26,27].

$$h^+ + SO_3^{2-} \rightarrow {}^\bullet SO_3^- \quad (4)$$

We have adopted the use of terephthalic acid (TPA) as a fluorescence probe to detect the ${}^\bullet OH$. The 0.025 g of Na_2SO_3 and 0.1 g of g-C_3N_4 were added into 200 mL aqueous solution of terephthalic acid (0.166 g) and NaOH (0.16 g). After 30 min visible light irradiation ($\lambda \geq 420$ nm), the fluorescence peak at 425 nm can be detected due to formation of 2-hydroxyterephthalic acid as a result of the reaction between terephthalic acid and ${}^\bullet OH$ (Fig. 2B) [28], confirming that the ${}^\bullet OH$ formed during the light irradiation. Obviously, the photoluminescence peak intensity of mixing suspension of g-C_3N_4 and Na_2SO_3 is higher than that of the g-C_3N_4 suspension, indicating that adding the Na_2SO_3 into the g-C_3N_4 suspension can promote the formation of ${}^\bullet OH$. Combining with the EPR results and fluorescence observation, we can conclude that a possible formation process of ${}^\bullet OH$ for light irradiation of Na_2SO_3 and g-C_3N_4 suspension is as follows: the SO_3^{2-} was firstly oxidized by photogenerated hole on g-C_3N_4 into ${}^\bullet SO_3^-$. Subsequently, ${}^\bullet SO_3^-$ radical is easy to react with dissolved oxygen and gives rise to the formation of the oxygen-centered peroxymonosulfate radical (${}^-O_3SOO^\bullet$) and sulfate radicals (${}^\bullet SO_4^-$) by chain propagation reaction steps rapidly. The ${}^\bullet OH$ may be generated *via* the reaction of ${}^\bullet SO_4^-$ with H_2O [29,30], as described in Eqs. (5)–(7). The white precipitation can be observed by adding the $BaCl_2$ into the suspension of Na_2SO_3 and g-C_3N_4 after 1 h light irradiation, indicating that the SO_3^{2-} was oxidized into SO_4^{2-} in the photocatalytic reaction *via* that process described by Eq. (6).

$${}^\bullet SO_3^- + O_2 \rightarrow {}^-O_3SOO^\bullet \quad (5)$$

$${}^\bullet O_3SOO^- + SO_3^{2-} \rightarrow SO_4^{2-} + {}^\bullet SO_4^- \quad (6)$$

$${}^\bullet SO_4^- + H_2O \rightarrow HSO_4^- + {}^\bullet OH \quad (7)$$

In order to further confirm that the SO_3^{2-} oxidation by hole takes part in the formation of ${}^\bullet OH$, ethanol was used to take the place of water. In the solvent of ethanol without supplied H^+ and OH^-, therefore it is impossible to occur for producing ${}^\bullet OH$. Under

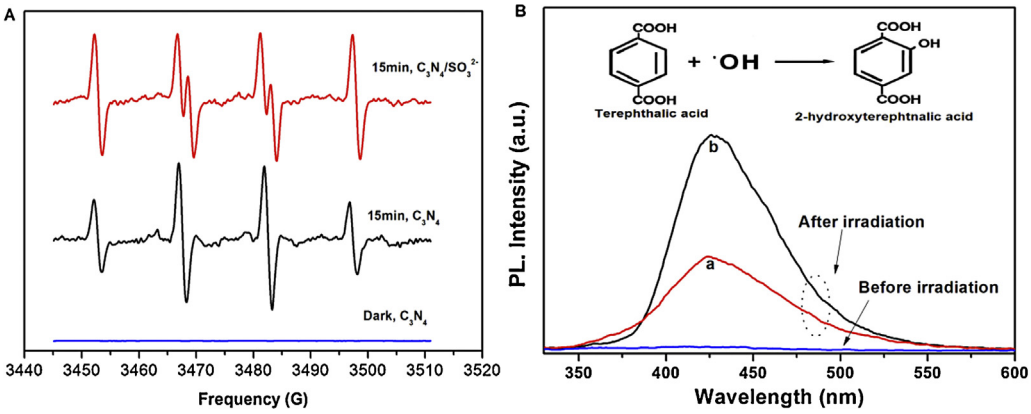

Fig. 2. (A) EPR spectra for the DMPO-containing g-C_3N_4 suspensionandNa_2SO_3 + g-C_3N_4 suspension, recorded after 15 min under visible light irradiation were initiated. (B) Photoluminescence spectra for the 20 mM NaOH + 5 mM TPA + g-C_3N_4 (curve a) and the 20 mM NaOH + 5 mM TPA + g-C_3N_4 + Na_2SO_3 (curve b) under visible light irradiation ($\lambda \geq 420$ nm) for 30 min.

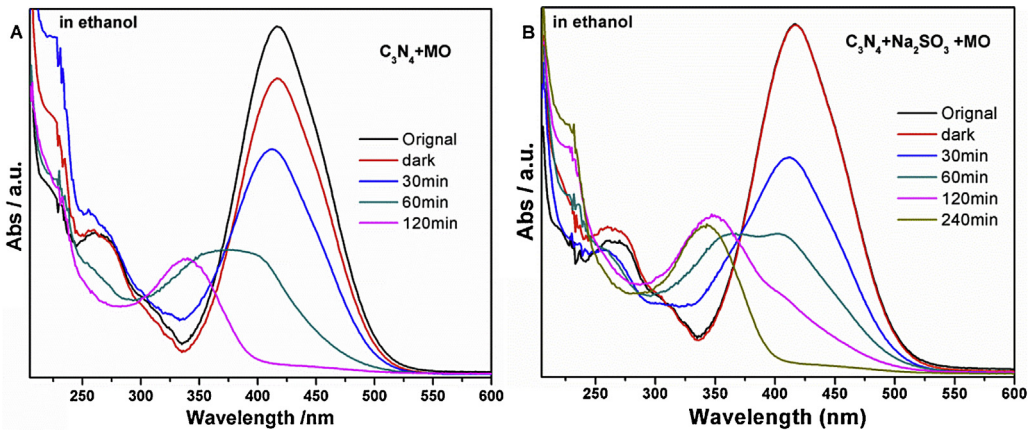

Fig. 3. UV–vis spectroscopic changes for MO over g-C_3N_4 in ethanol under air atmosphere absent (A) and present (B) Na_2SO_3.

visible light irradiation, the fading of MO would mainly originated from $^{\bullet}O_2^-$ oxidation due to the $^{\bullet}O_2^-$ radicals attacked preferentially aromatic rings with low electronic density (as deactivated aromatic rings in MO) [31]. As can be seen from Fig. 3, the photofading of MO was suppressed obviously by Na_2SO_3 in ethanol. This means that as described in Eqs. (5) and (6), the series of reactions to produce $^{\bullet}SO_4^-$ initiated from hole oxidation of Na_2SO_3 consume the dissolved oxygen, which process decreases the concentration of $^{\bullet}O_2^-$ species, thus decreasing the rate of MO degradation. The slow MO degradation in the SO_3^{2-} + ethanol also clearly indicates that the SO_3^{2-} oxidation by hole does not proceed to produce the $^{\bullet}OH$ in the presence of H_2O.

It is obvious that the oxygen is important for the formation of $^{\bullet}OH$. To check the effect of O_2 on the MO conversion, an experiment, visible light irradiation of MO-containing aqueous suspensions of g-C_3N_4, was carried out in Ar atmosphere. After 4 h light irradiation, the 42% decrease in absorbance peak intensity (at 464 nm, which caused by a conjugated structure formed by the azo bond under the strong influence of the electron-donating dimethylamino group [32]) of MO was achieved, while a new absorbance peak at 247 nm occurs (Fig. 4A). The redox potential of MO was 1.48 V *vs* NHE [33], which is slightly lower than oxidation potential (1.53 V) of valance band of g-C_3N_4. This fact does not support that the decrease in absorbance peak intensity of MO resulted from the hole oxidation process due to the low driving force. The new absorbance maximum at 247 nm would indicate that the MO is converted into a novel species. Indeed, as the reported by Fan et al. that sulfanilic acid with the absorption maximum at 247 nm can be engendered by the cleavage of the azo bond of MO in the absence of oxygen [34]. In our investigation, the same production is presented that reveals the hydrocracking reaction of the azo bond (—N=N—) of MO happens under the absence of oxygen. The reaction is according to

$$e^- + H_2O \rightarrow {}^{\bullet}H + OH^- \quad (8)$$

$$4{}^{\bullet}H + NaO_3S{-}(C_6H_4){-}N{=}N{-}(C_6H_4){-}N(CH_3)_2 \rightarrow NaO_3S{-}(C_6H_4){-}NH_2 + H_2N{-}(C_6H_4){-}N(CH_3)_2 \quad (9)$$

Under the same condition, adding the 0.2×10^{-4} mol Na_2SO_3 into the mixing suspension of g-C_3N_4 and MO, the absorbance peak of MO disappears completely after 3 h light irradiation and the peak at 247 nm gradually increases with increasing the light irradiation time (Fig. 4B), meaning that the hydrocracking of the azo bond of MO was significantly promoted. The enhanced hydrocracking process would be attributed to the depletion of hole on g-C_3N_4 by SO_3^{2-} (Eq. (4)) which facilitates the reduction reactions (Eqs. (8) and (9)) by photogenerated electrons to proceed.

Under air atmosphere, the hydrocracking of azo bond also can be observed in the SO_3^{2-} containing g-C_3N_4 aqueous suspension (Fig. 5). After 1 h light irradiation of the mixing suspension of g-C_3N_4, Na_2SO_3 and MO, the amount of SO_4^{2-} for performing the experiment in air ambient (determining by adding $BaCl_2$ to produce $BaSO_4$ precipitate) is much higher than similar experiment performed in Ar (Fig. S2). This fact confirms that the production of $^{\bullet}OH$ and $^{\bullet}SO_4^-$ during the photoreaction is a process of consuming dissolved oxygen, which process will induce an oxygen-poor environment in reaction solution. An authentic fact is that the hydrocracking reaction is easy to occur under an oxygen poor

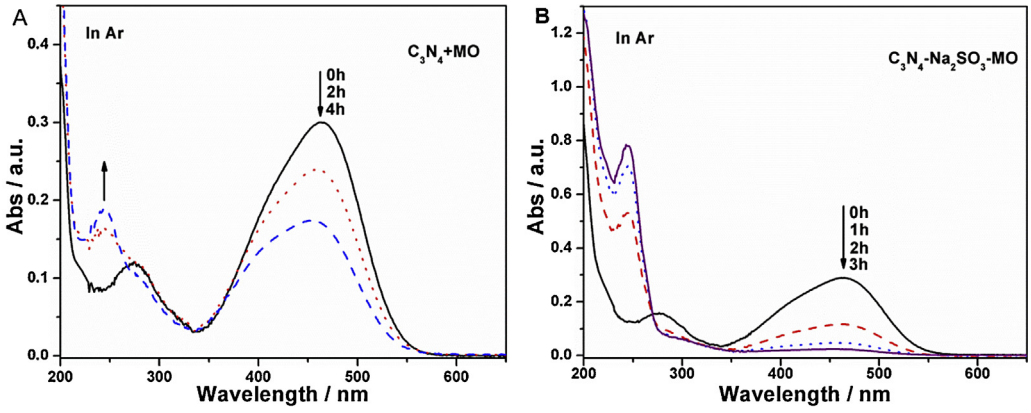

Fig. 4. UV–vis spectroscopic changes for MO over g-C_3N_4 in different solutions under Ar atmosphere, (A) in the deionized water, (B) in Na_2SO_3 solution.

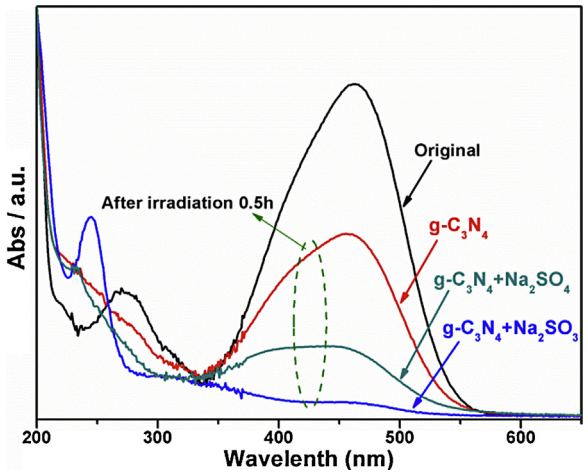

Fig. 5. UV–vis spectroscopic of MO photodegradation before and after irradiation for 0.5 h under different system.

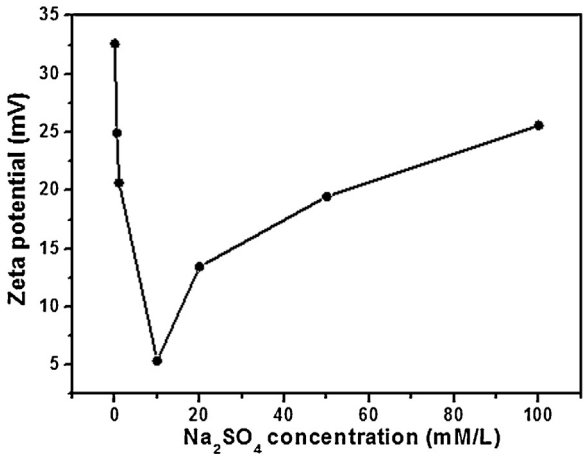

Fig. 6. The Zeta potential of g-C_3N_4 particles in the Na_2SO_4 solution with various concentrations.

environment [35]. Therefore, coexistence of g-C_3N_4 and SO_3^{2-} will induce the hydrocracking of MO to occur in the air atmosphere due to the oxygen-poor environment from the oxidation of SO_3^{2-}, significantly contributing to the rapid fading of MO.

Intelligibly, there are two complementary reactions under coexistence of g-C_3N_4 and SO_3^{2-}: (i) the photogenerated electron induced multistep reduction of O_2 into $^{\bullet}OH$, (ii) $^{\bullet}SO_4^-$ radical produced by a chain reaction originated from the hole oxidized SO_3^{2-} into $^{\bullet}SO_3^-$ and the $^{\bullet}OH$ further forms by $^{\bullet}SO_4^-$ reaction with H_2O as described by Eqs. (4)–(7). Thus, the two reaction processes promoted each other due to the increase in separation of photogenerated electron and hole when the either process occurs. Therefore, the faster decolorization process in the mixing solution of g-C_3N_4, Na_2SO_3 and MO shown in Fig. 1 would come from a combination effect of photodegradation and hydrocracking. Indeed, in the absence of Na_2SO_3, no hydrocracking of MO over g-C_3N_4 was observed under light irradiation (Fig. 5).

It should be pointed out that both the hydrogenation and degradation of MO will depend on the yield rate of photogenerated electrons in g-C_3N_4. An interesting is to understand the photogenerated carrier separation and transport in the g-C_3N_4 in the presence of ions. To understand effect of the Na^+ cation on photoactivity of g-C_3N_4, the Na_2SO_4 for substitution of Na_2SO_3 was added into the mixing solution of g-C_3N_4 and MO because the SO_4^{2-} is a chemically stable species under light irradiation. The MO is photodegraded completely in the g-C_3N_4 + Na_2SO_4 system in the 1.33 h light irradiation (Fig. 1), which is much faster than the photodegraded 66% of MO over g-C_3N_4 in the same light irradiation time. To further confirm the enhanced photoactivity of g-C_3N_4 by Na^+, the NaCl substituting for Na_2SO_4 with the same Na^+ concentration was added into the reaction solution. The photodegradation rate of MO over g-C_3N_4 in the NaCl solution is similar to that in Na_2SO_4 solution (Fig. 1). This fact may support a viewpoint that the photodegradation rate of dye is dependent on the Na^+ and the anions such as Cl^- and SO_4^{2-} do not affect the photoactivity of g-C_3N_4. The Zeta potential is a useful indicator to show the effect of ions on surface electrokinetic potential of particles in suspension. As shown in Fig. 6, the zeta potential was changed with increasing Na_2SO_4 concentration, implying that there is the interaction between ions and surface of g-C_3N_4. The zeta potential upon the addition of salt can be elaborated using the electric double layer theory which provides a quantitative understanding of the surface-charge development process for adsorption of aqueous ions onto the surface of the g-C_3N_4. The cation, Na^+, interacts with negatively charged nitrogen pots of g-C_3N_4 surface, and the counter SO_4^{2-} anions enter the stern layer of g-C_3N_4 suspension particles. Thus, the zeta potential decreases with increase of Na_2SO_4 concentration. The ion interaction with the surface of g-C_3N_4 reaches to saturation when the concentration of Na_2SO_4 more than 10 mM, and the zeta potential of g-C_3N_4 particles increase with the increase of Na_2SO_4 concentration. This evidence indicates that the effect of Na^+ ions on the photo excited g-C_3N_4 is a possible reason for the degradation of MO promoted by Na_2SO_4.

As shown in Fig. 7A, a large nitrogen pots in plane of g-C_3N_4 is composed of 3-fold N-bridge linking the triazine units, where are filled with six nitrogen lone-pair electrons (nitrogen pots) potentially ideal sites for metal inclusion. Indeed, it has been demonstrated that the metal ions are inclined to coordinate into the nitrogen pots in the plane of carbon nitride by the interaction between metal ions and negatively charged nitrogen atoms [36,37]. The diameter of nitrogen pots in g-C_3N_4 is about 0.477 nm, larger than ionic diameters of Na^+ (0.19 nm) [37]. Such large space which allows the Na^+ cations coordinate into the nitrogen pots by forming ion-dipole interaction with negatively charged N atoms, as demonstrated in K^+ or Na^+ coordinating into the polyether ring of 18-crown-6 [38]. The charge balance for Na^+ coordinating into the nitrogen pots of carbon nitride can be kept by forming the coordination bonds between Na^+ and negatively charged nitrogen atoms and SO_4^{2-}. Such structure would improve charge-separation and transport properties similar to the graphite intercalation compound [39]. In our previous report [40], it has been well confirmed that the Na^+ can coordinate to the nitrogen pots of g-C_3N_4 by intercalation by heating g-C_3N_4 in the Na-containing flux. The theoretical calculations have indicated that the Na^+ coordination to the nitrogen pots of g-C_3N_4 sheet will induce the distortion of the tri-s-triazine C_3N_4 layers [40]. As a result of the distortion, the charge distributions in the g-C_3N_4 sheet are changed from the relative uniform state to the un-uniform state, indicating that the build-in electric field forms by Na^+ coordination, which is useful to separation of the photogenerated electrons and holes. However, in this case, different to the Na^+ intercalation carbon nitride, the Na^+ only coordinates into the nitrogen pots on the surface of g-C_3N_4 *via* an ion-dipole interaction. Such an ion adsorption on the surface of g-C_3N_4 will probably induce the interfacial electric field to form, which enhances the photogenerated electron–hole separation efficiency and lifetime of the photogenerated electrons. A similar effect was observed in the Ag or Ag^+ modified g-C_3N_4 [41].

To confirm that the Na^+ can affect the charge separation and transfer in g-C_3N_4 sheet, the g-C_3N_4 powder was dispersed into the saturated Na_2SO_4 solution for 2 h, and then separated by centrifugation, dried at 100 °C for 10 h and such obtained sample was

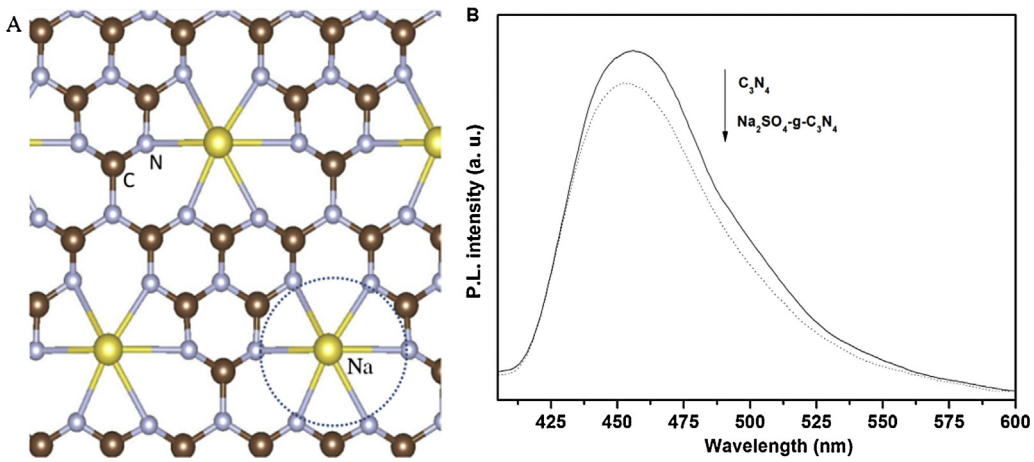

Fig. 7. (A) Schematic diagram of a perfect graphitic carbon nitride sheet constructed from tri-s-triazine units. (○) Indicates the nitrogen pots which filled with six nitrogen lone-pair electrons potentially ideal sites for metal inclusion. (B) Photoluminescence spectra for the g-C_3N_4 and the g-C_3N_4 after soaking treatment in Na_2SO_4 solution.

denoted as Na_2SO_4–g-C_3N_4. The photoluminescence (PL) spectrum for the Na_2SO_4–g-C_3N_4 sample as compared with the pure g-C_3N_4 is shown in Fig. 7B. The pure g-C_3N_4 showed the higher fluorescence intensity than Na_2SO_4–g-C_3N_4. For providing more information, we performed the time resolved fluorescence measurements. Fluorescence lifetimes extracted from the decay curves. In accordance with the steady state PL spectra, the fluorescence lifetime decreased from 4.99 ns for the g-C_3N_4 down to 4.30 ns for the Na_2SO_4–g-C_3N_4. This is due to an increased nonradiative rate (K_{nr}), that is, K_{nr} = 0.18 and 0.21 ns^{-1} for g-C_3N_4 and the Na_2SO_4–g-C_3N_4, respectively. The quenching of the emission intensity and its lifetime indicate that the relaxation of C_3N_4 exciting occurs *via* non-radiative paths, presumably by charge transfer of electrons and holes to new localized states which were formed by Na^+ ion coordination. The new charge transfer paths can be an indication for the photoactivity of materials.

To realize the reaction products concerning MO degradation, the total organic carbon (TOC) was observed (Table S1) and the intermediate products were determined by LC/MS (Fig. S3). After 30 min light irradiation, the TOC removal reaches to 69% in Na_2SO_3 + g-C_3N_4 suspension, which is significantly higher than those in g-C_3N_4 suspension (6.9%) and in Na_2SO_4 + g-C_3N_4 (21.9%) in the same light irradiation time. This demonstrated that Na_2SO_3 facilitates the degradation of MO. It is worth pointing out that the 69% TOC removal indicates that the MO was not mineralized completely, and the fading of MO occurred due to the hydrocracking of MO when coexistence of Na_2SO_3 and g-C_3N_4. As shown in Fig. 8, the LC/MS analysis showed that for MO photodegradation over g-C_3N_4 the possible degradation route is as follows: firstly, it involves the homolytic cleavage of the nitrogen–carbon bond of the amine group leading to the substitution of methyl group with a hydrogen atom [32]. Such a process seems to happen easily and gives rise to by-product ***1*** (m/z = 290). Subsequently, degradation of MO proceeds *via* two possible routes. The one route is that the sulfonic attached to benzene ring is substituted by a hydroxyl radical while the methyl amino group breaks off from the benzene ring (by-product ***2***, m/z = 198). Another route is the cleavage of azo bond connecting to two aromatic rings symmetric and to form the sulfanilic acid (by-product ***3***, m/z = 173) or by-product ***4*** (m/z = 157) [32]. The similar MO degradation process was found in the g-C_3N_4 + Na_2SO_3 system. The obvious difference is that in the g-C_3N_4 + Na_2SO_3 system only the single benzene containing products such as by-products ***5*** (m/z = 119), ***6*** (m/z = 217), and ***7*** (m/z = 261) were detected. The TOC and LC/MS results suggest that MO has been decomposed but not mineralized completely. The faster MO conversion and removal rates in g-C_3N_4 + Na_2SO_3 system than those in g-C_3N_4

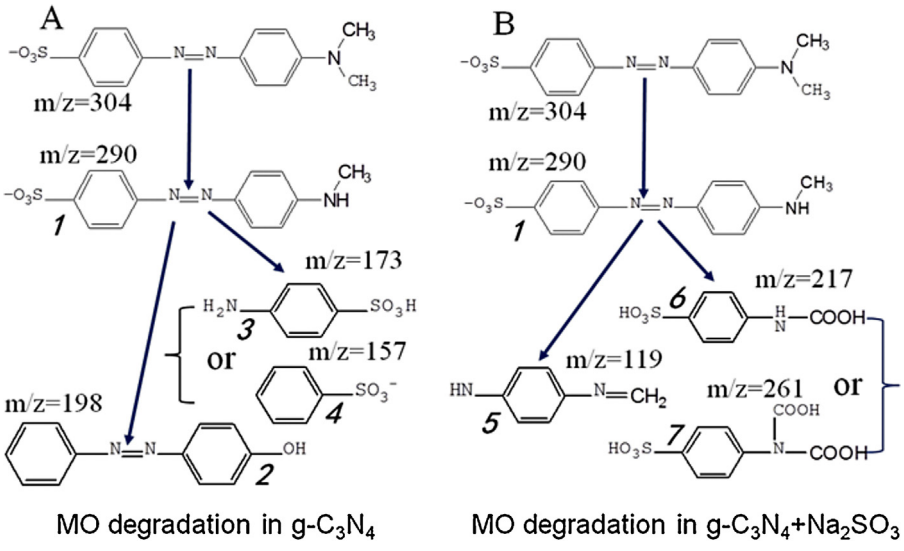

Fig. 8. The proposed photodegradation pathways for MO in g-C_3N_4 suspension without (A) and with Na_2SO_3 (B).

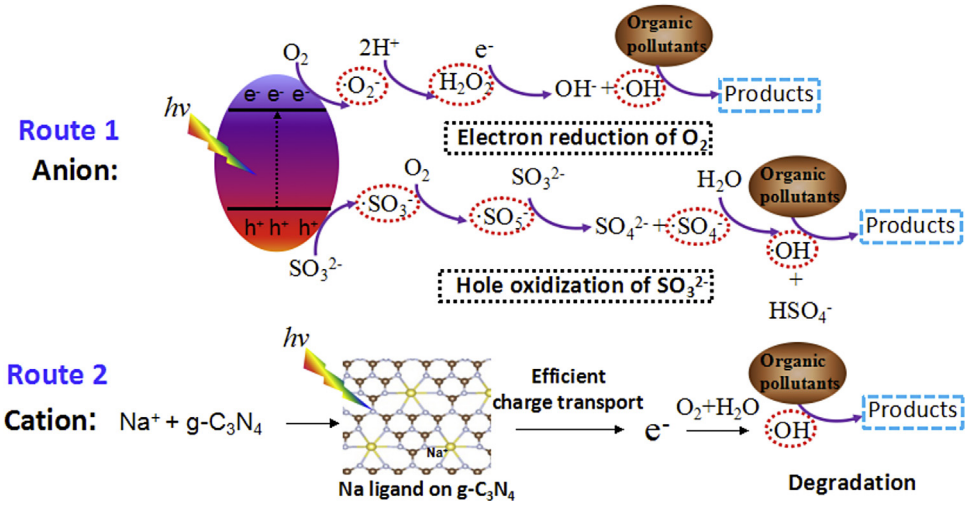

Fig. 9. Illustration of the promoted effect of SO_3^{2-} anion and Na^+ cation on the conversion of organic pollutants over g-C_3N_4 under visible light irradiation. The photogenerated hole of g-C_3N_4 on the valence band oxidized SO_3^{2-} into $^{\bullet}SO_3^-$ and then induced a chain reaction to produce $^{\bullet}OH$ while the photogenerated electron on the conduction band reduced O_2 to $^{\bullet}OH$ (Route 1). The coordination of Na^+ into the C—N sheets of g-C_3N_4 contributes to the enhancement in reducing species (electron) inducing the photodegradation of organic pollutants (Route 2).

system would originate from the increased concentration of $^{\bullet}OH$ by addition of Na_2SO_3.

We further choose several typical pollutions such as acid orange 7 (AO7), alizarin red (AR) and phenol, as degrading target to confirm the enhancement effect of Na_2SO_3 on g-C_3N_4 photocatalysis. The experimental results indicated that the degradation of AO7, AR and phenol was accelerated by coexistence of Na_2SO_3 and g-C_3N_4 (Figs. S4–S6). The enhanced degradation rate of organic pollutants would be attributed to the formation of high concentration of $^{\bullet}OH$, which can non-selectively react with almost all the organic compounds due to its high redox potential of 2.7 V *vs* NHE. These evidences further demonstrated that coexistence of Na_2SO_3 and g-C_3N_4 can efficiently improves the photoactivity of g-C_3N_4.

4. Conclusion

To summarize, as shown in Fig. 9, we have demonstrated that the Na_2SO_3 significantly promotes the photodegradation of organic dyes over g-C_3N_4 due to three major reasons: firstly, the photogenerated holes oxidize the SO_3^{2-} into $^{\bullet}SO_3^-$, and then induced a chain reaction for production of active species such as $^{\bullet}OH$. Secondly, the consumption of h^+ by SO_3^{2-} caused the increase in the concentration of photogenerated electron which accelerated the formation of $^{\bullet}OH$ *via* multistep reduction of O_2. In addition, the cation, Na^+, may interact with negatively charged nitrogen atoms in nitrogen pots of g-C_3N_4. Such interaction reduced fluorescence intensity and lifetime, indicating the formation of new, non-radiative deactivation pathways, involving charge-transfer processes. The improved charge transport properties significantly enhance the formation of active species, thus improving the photodegradation of organic pollutants. Our studies offer the new opportunities for using the g-C_3N_4 with low cost and facile adjustable function to treat industrial wastewater containing organic pollutants. Moreover, the consumption of sulfite during the g-C_3N_4 photocatalysis also provides a useful method for capture and removal of SO_2.

Acknowledgments

This work was funded by the National Basic Research Program of China (973 Program, 2013CB632404) and the National Natural Science Foundation of China (Nos. 51102132, 11174129, 51272101, and 51272102).

Appendix A. Supplementary data

Structure information of g-C_3N_4 with ABA stacking of graphene-like C-N conjugated sheet, change of TOC for different systems before and after photocatalytic reaction, Negative ion ESI mass spectra for intermediate and final products from MO degradation over different system, and the effect of sodium sulfite for the photodegradation to some other organic dyes.

Supplementary data associated with this article can be found, in the online version, at http://dx.doi.org/10.1016/j.apcatb.2014.04.036.

References

[1] C. Chen, W. Ma, J.C. Zhao, Chem. Soc. Rev. 39 (2010) 4206–4219.
[2] M. Pelaez, N.T. Nolan, S.C. Pillai, M.K. Seery, P. Falaras, A.G. Kontos, P.S.M. Dunlop, J.W.J. Hamilton, J.A. Byrne, K. O'Shea, M.H. Entezari, D.D. Dionysiou, Appl. Catal. B: Environ. 125 (2012) 331–349.
[3] M. Tanveer, G.T. Guyer, Renew. Sustain. Energy Rev. 24 (2013) 534–543.
[4] L.G. Devi, R. Kavitha, Appl. Catal. B: Environ. 140–141 (2013) 559–587.
[5] K. Maeda, K. Teramura, L. Daling, T. Takata, N. Saito, Y. Inoue, K. Domen, Nature 440 (2006) 295–296.
[6] X.C. Wang, K. Maeda, A. Thomas, K. Takanabe, G. Xin, J.M. Carlsson, K. Domen, M. Antonietti, Nat. Mater. 8 (2009) 76–80.
[7] Z. Huang, F. Li, B. Chen, T. Lu, Y. Yuan, G. Yuan, Appl. Catal. B: Environ. 136–137 (2013) 269–277.
[8] Y. Wang, X.C. Wang, M. Antonietti, Angew. Chem. Int. Ed. 51 (2012) 68–89.
[9] W. Shen, W. Fan, J. Mater. Chem. A 1 (2013) 999–1013.
[10] Y. Zheng, J. Liu, J. Liang, M. Jaroniec, S.Z. Qiao, Energy Environ. Sci. 5 (2012) 6717–6731.
[11] G. Liu, P. Niu, C. Sun, S.C. Smith, Z. Chen, G.Q. Lu, H.M. Cheng, J. Am. Chem. Soc. 132 (2010) 11642–11648.
[12] S.C. Yan, S.B. Lv, Z.S. Li, Z.G. Zou, Dalton Trans. 39 (2010) 1488–1491.
[13] S. Min, G. Lu, J. Phys. Chem. C 116 (2012) 19644–19652.
[14] M. Zhang, J. Xu, R. Zong, Y. Zhu, Appl. Catal. B: Environ. 147 (2014) 229–235.
[15] J. Sun, J. Zhang, M. Zhang, M. Antonietti, X. Fu, X. Wang, Nat. Commun. 3 (2012) 1139, http://dx.doi.org/10.1038/ncomms2152.
[16] M.N. Chong, B. Jin, C.W.K. Chow, C. Saint, Water Res. 44 (2010) 2997–3027.
[17] S.T. Martin, A.T. Lee, M.R. Hoffmann, Environ. Sci. Technol. 29 (1995) 2567–2573.
[18] M. Liu, Z. Lin, J.M. Lin, Anal. Chim. Acta 670 (2010) 1–10.
[19] L. Kylhammar, P.A. Carlsson, M. Skoglundh, J. Catal. 284 (2011) 50–59.
[20] S.C. Yan, Z.S. Li, Z.G. Zou, Langmuir 25 (2009) 10397–10401.
[21] T.X. Wu, T. Lin, J.C. Zhao, H. Hidaka, N. Serpone, Environ. Sci. Technol. 33 (1999) 1379–1387.
[22] S.C. Yan, Z.S. Li, Z.G. Zou, Langmuir 26 (2010) 3894–3901.
[23] G.G. Liu, X.Z. Li, J.C. Zhao, S. Horikoshi, H. Hidaka, J. Mol. Catal. A: Chem. 153 (2000) 221–229.
[24] K. Ranguelova, S. Chatterjee, M. Ehrenshaft, D.C. Ramirez, F.A. Summers, M.B. Kadiiska, R.P. Mason, J. Biol. Chem. 285 (2010) 24195–24205.
[25] P. Neta, R.E. Huie, A.B. Ross, J. Phys. Chem. Ref. Data 17 (1988) 1027–1284.

[26] S.H. Hsieh, G.J. Lee, C.Y. Chen, J.H. Chen, S.H. Ma, T.L. Horng, K.H. Chen, J.J. Wu, J. Nanosci. Nanotechnol. 12 (2012) 5930–5936.
[27] M.A. holmes, T.K. Townsend, F.E. Osterloh, Chem. Commun. 48 (2011) 371–373.
[28] K. Ishibashi, A. Fujishima, T. Watanabe, K. Hashimoto, Electrochem. Commun. 2 (2000) 207–210.
[29] C. Mottley, R.P. Mason, Arch. Biochem. Biophys. 267 (1988) 681–689.
[30] M.J. Davies, B.C. Gilbert, J.K. Stell, A.C. Whitwood, J. Chem. Soc., Perkin Trans. 2 (1992) 333–335.
[31] L. Cermenati, P. Pichat, C. Guillard, A. Albini, J. Phys. Chem. B 101 (1997) 2650–2658.
[32] J. Fan, Y. Guo, J. Wang, M. Fan, J. Hazard. Mater. 166 (2009) 904–910.
[33] F. Chen, Z.G. Deng, X.P. Li, J.L. Zhang, J.C. Zhao, Chem. Phys. Lett. 415 (2005) 85.
[34] R. Comparelli, E. Fanizza, M.L. Curri, P.D. Cozzoli, G. Mascolo, R. Passino, A. Agostiano, Appl. Catal. B: Environ. 55 (2005) 81–91.
[35] G. Brown, A.R. Darwent, J. Chem. Soc., Faraday Trans. 1 80 (1984) 1631–1643.
[36] X.C. Wang, X.F. Chen, A. Thomas, X.Z. Fu, M. Antonietti, Adv. Mater. 21 (2009) 1609–1612.
[37] S. Barman, M. Sadhukhan, J. Mater. Chem. 22 (2012) 21832–21837.
[38] C.J. Pedersen, J. Am. Chem. Soc. 89 (1967) 7017–7036.
[39] M.S. Dresselhaus, G. Dresselhaus, Adv. Phys. 51 (2002) 1–186.
[40] H.L. Gao, S.C. Yan, J.J. Wang, Y.A. Huang, P. Wang, Z.S. Li, Z.G. Zou, Phys. Chem. Chem. Phys. 15 (2013) 18077–18084.
[41] Y. Bu, Z. Chen, W. Li, Appl. Catal. B: Environ. 144 (2014) 622–630.